Dissociation pathways and binding energies of lithium clusters from evaporation experiments

C. Bréchignac, H. Busch, Ph. Cahuzac, and J. Leygnier

Citation: J. Chem. Phys. **101**, 6992 (1994); doi: 10.1063/1.468326
View online: http://dx.doi.org/10.1063/1.468326
View Table of Contents: http://jcp.aip.org/resource/1/JCPSA6/v101/i8
Published by the AIP Publishing LLC.

Dissociation pathways and binding energies of lithium clusters from evaporation experiments

C. Bréchignac, H. Busch,[a] Ph. Cahuzac, and J. Leygnier
Laboratoire Aimé Cotton, CNRS II, Campus d'Orsay Bât. 505, 91405 Orsay Cedex, France

(Received 16 February 1994; accepted 6 July 1994)

The unimolecular dissociation of energy rich lithium cluster ions shows that Li_n^+ dissociate by sequential atom or dimer loss. The binding energies of Li_n^+ ($n=4-42$) generated in an evaporative ensemble are determined from unimolecular decay, within a well defined time window, and energy constraint. They present a sawtooth behavior vs cluster size less pronounced that it should be from a simple metal model. Odd–even alternation is superimposed on the sawtooth behavior, with odd sized cluster ions being more stable. Cohesive energies per atom of Li_n^+ are deduced from these dissociation energies up to $n=40$ and from extended photo-induced measurements up to $n=95$. Cohesive energies per atom of neutral clusters Li_n are derived by combining these ionic cohesive energies with the literature ionization potentials. The linearity of the neutral cluster cohesive energy vs the cluster surface to volume ratio permits a volume and a surface energy to be deduced. These values are compared to the bulk values.

I. INTRODUCTION

For a long time, the fragmentation of finite systems has been considered as the main tool to probe their binding strength. Recently, investigations of dissociation phenomena in free atomic or molecular clusters have been successfully used to study cluster stability. In most cases, neutral and singly charged clusters are intrinsically stable and their dissociation is endothermic. Hence an excess of energy is necessary to promote dissociation. This has been achieved either in collision or in photoabsorption experiments.

In general, after its excitation, the internal energy is statistically distributed among the numerous vibrational modes of the system and the cluster does not instantaneously dissociate. The concept that there is a delay between excitation of a finite system and its subsequent dissociation is not new and was suggested in the 1920s as the "unimolecular decomposition." In fact the dynamics of unimolecular dissociation in finite systems reveals the influence of internal energy content and mode number on the dissociation mechanism.[1] Statistical models of energy partitioning permit the determination of binding energy from kinetic energy release or from the dissociation rate within a well defined time interval provided that internal energy is well known. In cluster experiments a basic difficulty in the binding energy determination is the wide distribution of internal energy of the ensemble of cluster parents which depends on cluster preparation.[2] One possibility to partially overcome this problem is to study the unimolecular dissociation of clusters formed from an *evaporative ensemble*.[3] However for an evaporative ensemble, the evaporation rates of different cluster sizes remain unchanged if all the dissociation energies are scale by the same factor. In order to obtain absolute values for the binding energies vs cluster size an energy constraint is required.

There have been several previous studies of the dissociation energies of atomic and molecular clusters showing appreciable change from the corresponding bulk. It is then of particular interest to follow the binding energy of cluster as a function of the number of constituents in order to see to what extent the nature of the cluster bond evolves with size. Even if it is known that for small cluster sizes their properties depend rather irregularly upon cluster size, it is assumed that, for large enough clusters, properties converge smoothly to the infinite limit. Even though there is an increasing number of studies on dissociation energies of small clusters,[4] there is still a lack of information on larger clusters. Up to now, available data in the size range of one hundred atoms have been provided only for Na,[5] K,[6] Hg,[7] and Si.[8]

In this paper we report a dissociation study of lithium cluster ions containing up to 100 atoms. For cluster with less than 40 atoms we used the unimolecular dissociation of ionized cluster parents forming an evaporative ensemble. This method, previously used for small sodium and potassium cluster ions[4] is extended here to larger sizes for which two successive evaporative events can occur during the observational time window. For cluster ions with more than 40 atoms, we use a photoinduced evaporation method.[6] The deduced dissociation energies present a sawtooth behavior which is interpreted in terms of electronic shell structure and compared to the available calculations. The cohesive energies (i.e. energies per atom) for neutrals are derived from the dissociation energies of the ions and the literature ionization energies.[9] The linearity of the cluster cohesive energy versus the cluster surface to volume ratio permits a volume and a surface energy to be deduced. These values are compared to the bulk values.

II. EXPERIMENT

A schematic diagram of the experimental apparatus is shown in Fig. 1. The lithium clusters are formed by nucleation from the metal vapor in a He gas condensation cell cooled by liquid nitrogen. Clusters condensed out of the quenched vapor are carried out by the He gas stream in a copper tube of 7 cm length and 1.2 cm diameter ending with

[a]Present address: The Niels Bohr Institute, Blegdamsvej 17, 2100 Copenhagen, Denmark.

 0021-9606/94/101(8)/6992/11/$6.00

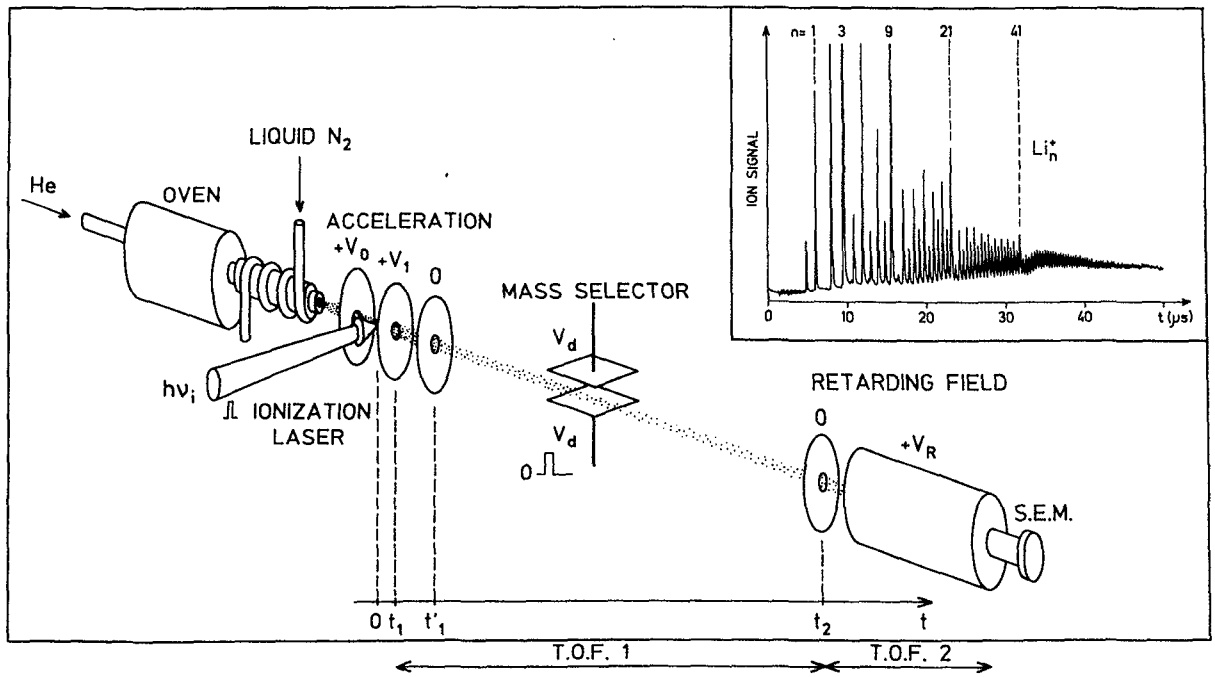

FIG. 1. Schematic diagram of the experimental apparatus. The origin of time is defined by the laser shot. The inset shows a mass spectrum of Li_n^+ (V_d=0) obtained at high laser fluence with no retarding field, i.e., V_R=0.

1.5–4 mm diam hole. The size distribution of the clusters is controlled by varying the He gas pressure, the oven temperature, and the hole diameter. As we have shown in a previous paper[10] that the neutral cluster size distribution has a Gaussian-type shape, the maximum of which shifts toward higher masses as the helium pressure is increased. We choose to start with a neutral distribution Li_n peaking at about n=900 with full-width at half-maximum of Δn=300, so that no appreciable number of clusters containing less than 100 atoms are produced. After passing through a differential pumping chamber, the neutral clusters are photoionized with a pulsed UV laser source within the ionizing region of a Willey McLaren-type time-of-flight spectrometer[11] and subject to a uniform acceleration field about 1000 V cm^{-1}. The energy of ionizing photon ($h\nu$=3.5 eV) permits direct photoionization. At high laser fluence, ionized clusters absorb multiple photons, greatly increasing the internal energy content of the cluster ions during the 10 ns duration of the ionizing laser pulse. Rapid sequential evaporations occur during the residence time t_1 in the ionizing region (1–3 μs) resulting in an ion cluster distribution shifted toward smaller masses (inset of Fig. 1). Such a distribution for which each cluster is the result of at least one evaporation constitutes an evaporative ensemble.[3] This ensemble of ion clusters is accelerated to a final ion beam energy of 5 keV. The acceleration duration $t'_1 - t_1$ (Fig. 1) is shorter than t_1 making evaporation in the accelerating region negligible. The accelerated ion clusters enter a field free drift tube where they spatially resolve into separated mass packets. By applying suitable electric pulses to the deflection plates of the mass selector located in the drift tube, a single mass packet can be selected. During their flight ($t_2 - t'_1$) parent cluster ions undergo further evaporation with parent and fragment particles proceeding at the center of mass velocity. A retarding field time of flight spectrometer mass analyses the selected packet at time t_2.

With this tandem time of flight spectrometer we studied the unimolecular dissociation, occurring during the time $t_2 - t'_1$, of a mass selected packet Li_n^+ formed from an "evaporative ensemble." It has to be noted that the acceleration duration $t'_1 - t_1$ is shorter than t_1, so that we use $t_2 - t_1$ instead of $t_2 - t'_1$ in the following.

III. EXPERIMENTAL RESULTS

An example of unimolecular spectrum is shown in Fig. 2. Trace (a) corresponds to the peak associated with the cluster packet Li_{21}^+ selected at t'_1 and observed with no retarding field. Trace (b) shows the ion peak intensities of Li_{21}^+, Li_{20}^+, and Li_{19}^+, clusters resulting from the unimolecular decay, of the parent packet Li_{21}^+, during their time of flight (t'_1,t_2), and dispersed by a 2000 V retarding field.

As already observed for Na_n^+ (Ref. 5) and K_n^+ clusters,[6] we find that Li_n^+ clusters with n ranging from 5 to 42 evaporate neutral species leading to Li_{n-1}^+ or Li_{n-2}^+ ionic fragments. We define the fractional dissociation ratios

$$F_{n,1}=\frac{S_{n-1}}{S_n+S_{n-1}+S_{n-2}}, \tag{1}$$

$$F_{n,2}=\frac{S_{n-2}}{S_n+S_{n-1}+S_{n-2}}, \tag{2}$$

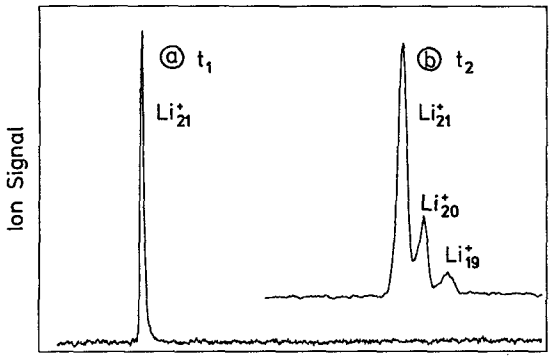

FIG. 2. Example of unimolecular dissociation. Trace (a) shows the mass selected parent packet with no retarding field. Trace (b) displays the dispersion of the mass selected packet with V_R=2000 volts showing the unimolecular dissociation during the time of flight $(t_2 - t_1')$.

$$F_n = \frac{S_{n-1} + S_{n-2}}{S_n + S_{n-1} + S_{n-2}}, \tag{3}$$

where S_n, S_{n-1}, and S_{n-2} are the Li_n^+, Li_{n-1}^+, and Li_{n-2}^+ peak areas of the remaining parents and of the ionic fragments, respectively.

The total unimolecular decay rate F_n of Li_n^+ clusters within the time window (t_1, t_2) is plotted in Fig. 3(a) vs n. It presents a general increase with cluster size, with local deviations around the mean trend. Figure 3(b) represents the branching ratio $F_{n,1}/F_n$ for the loss of one atom. Except for Li_6^+, Li_7^+, and Li_8^+, it shows an odd–even alternation, the amplitude of which decreases as cluster size increases. The experimental reproducibility is within 10%, and does not depend on the laser flux.

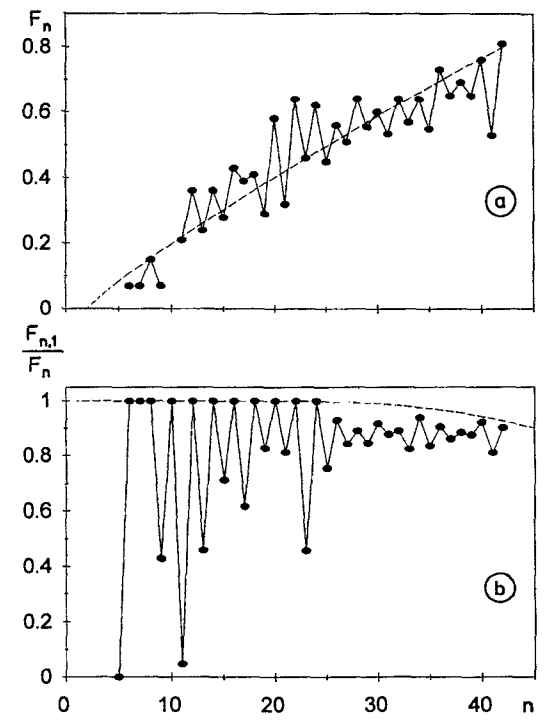

FIG. 3. Fractional dissociation ratios of Li_n^+ within the time $(t_2 - t_1')$ as a function of cluster size. Trace a compares the measured total decay F_n with the predicted decay from Eq. (22) which assumes a constant dissociation energy with cluster size. Trace (b) shows experimental ratios (dots) of Li_n^+ to total fragment intensities. The dashed line is the calculated ratio of one monomer to total (one+two monomers) fragment intensities. Deviations of the experimental data from the dashed line reflect the dimer evaporation.

For small cluster sizes ($n \leqslant 25$), the fractional dissociation ratio is lower than 50%–60%, and only one evaporation step occurs during (t_1, t_2) (see Sec. IV). The production of Li_{n-2}^+ ion fragments result from neutral dimer evaporation as experimentally characterized for the dissociation of K_5^+.[6] From Fig. 3(b) it is clear that even numbered Li_n^+ clusters evaporate only a monomer whereas odd numbered clusters lose either a monomer or a dimer, except for Li_7^+ which evaporates only a monomer.

For larger dissociation rates, a second evaporation step appears during the observational time window (t_1, t_2). The production of Li_{n-2}^+ from the parent Li_n^+ can also be due to the sequential loss of two monomers, as studied by Märk and co-workers on Ar_n^+ and $(N_2)_n^+$ clusters.[12] Consequently, the process $Li_n^+ \rightarrow Li_{n-2}^+$ in large clusters may result from the evaporation of a neutral dimer,

$$Li_n^+ \rightarrow Li_{n-2}^+ + Li_2 \tag{4}$$

and from the sequential evaporation of two neutral atoms,

$$Li_n^+ \rightarrow Li_{n-1}^+ + Li \rightarrow Li_{n-2}^+ + 2Li. \tag{5}$$

The branching ratio between these two channels will be discussed in Sec. IV.

IV. FROM UNIMOLECULAR DECAY TO DISSOCIATION ENERGIES

The unimolecular decay rates probe the dynamics of cluster evaporation. In order to interpret the experimental data one needs to know the cluster evaporation rate constants and, as these constants depend on cluster internal energy, the internal energy distribution of a mass selected cluster bunch.

For small ion clusters ($n \leqslant 25$), the dissociation energies of the monomer and dimer evaporation channels are deduced with the method we used for sodium and potassium clusters when only one evaporation step occurs during the experimental time window. For larger sizes, we present an extension of the method, in the case where clusters may undergo two successive evaporative events. This extension permits the dissociation energies of ionized lithium clusters Li_n^+ from n=5 to n=42 to be obtained.

A. Rate equations

In this section, we describe the evaporation dynamics of Li_n^+ initially containing the internal energy E. This energy is high enough, to promote either monomer or dimer evaporation during the observational time window, then each of the ionic fragments can also evaporate either a monomer or a

dimer, and so on.

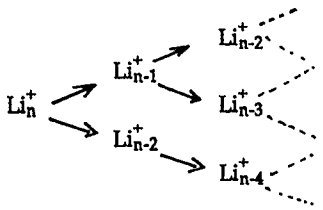

The distribution of fragments obtained at time t depends on the dynamics of the successive evaporative events. The internal energy of fragments decreases by about the dissociation energy at each step, hence the metastable lifetime increases.

Assuming a statistical treatment,[1] the metastable lifetime of small ion clusters increases by at least a factor of 10 between successive evaporations. Only one evaporation step within the observational time window is observed. The rate equations are

$$\begin{aligned}
&\frac{d}{dt}(\mathrm{Li}_n^+) = -k_n^{(1)}(\mathrm{Li}_n^+),\\
&\frac{d}{dt}(\mathrm{Li}_{n-1}^+)^{(1)} = k_{n,1}^{(1)}(\mathrm{Li}_n^+),\\
&\frac{d}{dt}(\mathrm{Li}_{n-2}^+)^{(1)} = k_{n,2}^{(1)}(\mathrm{Li}_n^+),
\end{aligned} \tag{7}$$

where $(\mathrm{Li}_{n-p}^+)^{(1)}$ represents the number of fragments at time t. Index (1) indicates that these fragments are the results of the first evaporation event. $k_{n,1}^{(1)}$ and $k_{n,2}^{(1)}$ are the partial rate constants for the evaporation of a monomer or a dimer, respectively, and $k_n^{(1)} = k_{n,1}^{(1)} + k_{n,2}^{(1)}$ is the total rate constant.

For larger clusters, the relative cooling at each step is less important so that the metastable lifetime slowly increases from one step to the next one. Two or more successive evaporation events occur during the time window (t_1', t_2). The equations for the formation of Li_{n-1}^+, Li_{n-2}^+, Li_{n-3}^+, and Li_{n-4}^+ become

$$\begin{aligned}
&\frac{d}{dt}(\mathrm{Li}_n^+) = -k_n^{(1)}(\mathrm{Li}_n^+),\\
&\frac{d}{dt}(\mathrm{Li}_{n-1}^+)^{(1)} = k_{n,1}^{(1)}(\mathrm{Li}_n^+) - k_{n-1}^{(2)}(\mathrm{Li}_{n-1}^+)^{(1)},\\
&\frac{d}{dt}(\mathrm{Li}_{n-2}^+)^{(1)} = k_{n,2}^{(1)}(\mathrm{Li}_n^+) - k_{n-2}^{(2)}(\mathrm{Li}_{n-2}^+)^{(1)},\\
&\frac{d}{dt}(\mathrm{Li}_{n-2}^+)^{(2)} = k_{n-1,1}^{(2)}(\mathrm{Li}_{n-1}^+)^{(1)},\\
&\frac{d}{dt}(\mathrm{Li}_{n-3}^+)^{(2)} = k_{n-2,1}^{(2)}(\mathrm{Li}_{n-2}^+)^{(1)} + k_{n-1,2}^{(2)}(\mathrm{Li}_{n-1}^+)^{(1)},\\
&\frac{d}{dt}(\mathrm{Li}_{n-4}^+)^{(2)} = k_{n-2,2}^{(2)}(\mathrm{Li}_{n-2}^+)^{(1)}.
\end{aligned} \tag{8}$$

Index (2) indicates that the ionic fragments are the result of two successive evaporative events.

This system can be generalized and solved analytically. For Li_n^+ existing at t_0, the probability to have no evaporation, one monomer, one dimer, or two monomer evaporations before time t are, respectively,

$$P_{t_0,t}(n,E,n) = \exp -k_n^{(1)}(t-t_0), \tag{9}$$

$$P_{t_0,t}^{(1)}(n,E,n-1) = \frac{k_{n,1}^{(1)}}{k_{n-1}^{(2)} - k_n^{(1)}}\left[\exp -k_n^{(1)}(t-t_0) - \exp -k_{n-1}^{(2)}(t-t_0)\right], \tag{10}$$

$$P_{t_0,t}^{(1)}(n,E,n-2) = \frac{k_{n,2}^{(1)}}{k_{n-2}^{(2)} - k_n^{(1)}}\left[\exp -k_n^{(1)}(t-t_0) - \exp -k_{n-2}^{(2)}(t-t_0)\right], \tag{11}$$

$$P_{t_0,t}^{(2)}(n,E,n-2) = k_{n,1}^{(1)}k_{n-1,1}^{(2)} \times \sum_{j=0}^{j=2} \frac{\exp -k_{n-j}^{j+1}(t-t_0)}{\Pi_{l=0,l\neq j}^{l=2}(k_{n-1}^{l+1} - k_{n-j}^{j+1})}. \tag{12}$$

It has to be noted that the evaporation rate constants depend strongly on the cluster internal energy, and that the clusters constituting a mass selected bunch may display a significant internal energy distribution. Comparison between calculated and measured fractional dissociation ratios should be done after integrating over the internal energy distribution of the mass selected packet.

B. Evaporative ensemble

The concept of *evaporative ensemble* has been developed by Klots.[3] It leads to an estimate of the internal energy distribution of each bunch of n-atom clusters.

The conditions required for a system of particles to form an evaporative ensemble born at t_0 and observed at a time t_1 are (i) Each particle dissipates its internal energy only by evaporation. Collision or radiative energy losses are supposed to be negligible. (ii) Each cluster existing at t_1 is the result of at least one evaporation.

We suppose that (i) is fulfilled and we discuss the validity of (ii) for the Li_n^+ cluster distribution, with $n=[1,100]$ obtained in our experimental conditions.

The size distribution of the ionized lithium clusters depends on the ionizing-warming laser fluence. At photon energies ($h\nu = 3.50$ eV), we vary the nucleation conditions in order to obtain, at low laser fluence, a cluster ion distribution peaking at $n=900$ atoms with half-width at half-maximum 300 atoms. We verify that clusters containing less than 100 atoms are not produced. By increasing the laser fluence, the ion distribution is shifted toward the low masses leading to smaller ion clusters, exclusively produced by evaporation of large masses so that condition (ii) is achieved. Hence, a collection of ion clusters Li_n^+ having n atoms contain a distribution of internal energy that is bracketed by the evaporation lifetimes. Assuming that the time spent in undergoing any evaporations prior to that of Li_{n+1}^+, is negligible as compared to t_1, the probability that Li_{n+1}^+ evaporates a monomer before t_1 to form Li_n^+ containing internal energy E is obtained from Eq. (10),

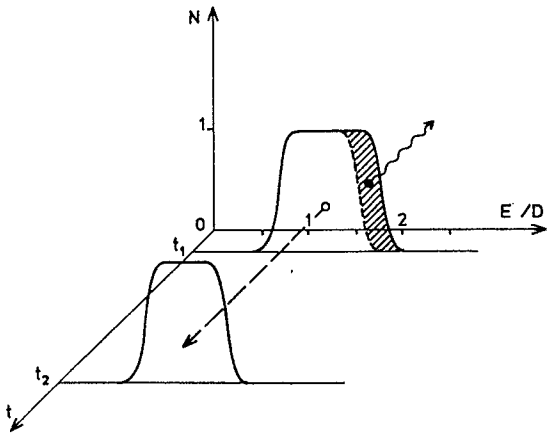

FIG. 4. Schematic distribution of internal energy of a mass selected cluster packet Li_n^+ at t_1 and t_2 assuming a time separation of evaporative events (valid for small sizes). The cross hatched area between the two curves represents the number of clusters which have undergone one evaporation during t_2-t_1.

$$P_n(E,t_1)=P_{n+1}(E+D,0)\,\frac{k_{n+1}(E+D)}{k_{n+1}(E+D)-k_n(E)}\{\exp -[k_n(E)t_1]-\exp-[k_{n+1}(E+D)t_1]\}, \quad (13)$$

$P_{n+1}(E+D,0)$ is the probability that Li_{n+1}^+ has the energy $E+D$ at $t_0=0$, and D is the dissociation energy of Li_{n+1}^+.

$P_n(E,t_1)$ describes the energy distribution of Li_n^+ at t_1 which is roughly square in shape. The high energy edge is approximately defined by

$$k_n(E_1)=1/t_1 \quad (14)$$

and the low energy edge by

$$k_{n+1}(E_1'+D)=1/t_1. \quad (15)$$

This indicates that Li_n^+ which contains more energy than E_1 evaporates before t_1 and that Li_{n+1}^+ which contains more energy than $E_1' + D$ forms Li_n^+ by evaporation before t_1. If the dissociation energies and the rate constants little vary with size $E_1 = E_1'$, the width of the energy distribution is D, as shown in Fig. 4.

The Li_n^+ cluster packet, with an energy distribution given by an evaporative ensemble isolated at t_1 will continue to evaporate after its mass selection. At t_2, clusters having highest energy have evaporated to lower masses. The energy distribution of the remaining clusters Li_n^+ at t_2 is narrower than the initial one at t_1. The low energy edge is unchanged. The high energy edge is approximately defined by

$$k_n(E_2)=1/t_2. \quad (16)$$

This simplification illustrated in Fig. 4 is valid if one assumes a time separation of the evaporative events. It implies that the evaporative lifetimes increase by one order of magnitude between successive evaporations, which may not be adequate for large cluster sizes.

C. Evaporative rate constants

The evaporative rate constants are derived from two well known statistical theories.

One is based on the concept of transition state. The simplest choice is the RRK classical expression,[13,14]

$$k_n(E)=\nu g\left(1-\frac{D_n}{E}\right)^{3n-7}, \quad (17)$$

where ν is the typical vibrational frequency of the particle, g is a degeneracy factor equal to the number of surface atoms for monomer evaporation, and D_n the dissociation energy of a n atom cluster. It tends in large n limit to the Arrhenius law

$$k_n(E)=\nu g\,\exp\left(-\frac{D_n}{kT}\right), \quad (18)$$

where T is the temperature of the cluster defined as a microcanonical ensemble $kT=E/(3n-6)$. A more sophisticated treatment (RRKM theory) requires the knowledge of the density of states at the transition state.[15]

The other, the phase space theory based on the microreversibility principle, has been developed by Weisskopf for nuclear reactions[16] and leads to

$$k_n(E)=S\nu^3\,\frac{3n-7}{E}\,8\pi m\left(1-\frac{D_n}{E}\right)^{3n-8}, \quad (19)$$

where S is the geometrical cluster cross section and m the reduced mass of the ejected atom.

D. Determination of cluster binding energies

For sake of simplicity we first use monomer evaporating rate constants deduced from the Arrhenius law, even for small masses. The fractional dissociation ratio F_n associated to the evaporation of Li_n^+ during the time window (t_2-t_1) is

$$F_n=\frac{E_1-E_2}{E_1-(E_1'-D_{n+1})}. \quad (20)$$

From Eqs. (14), (16), and (18) one obtains assuming $g=n$ for small sizes,

$$F_n=\frac{(3n-6)\left[\frac{1}{\ln(t_1\nu n)}-\frac{1}{\ln(t_2\nu n)}\right]}{\frac{3n-6}{\ln(t_1\nu n)}-\frac{D_{n+1}}{D_n}\left\{\frac{3n-3}{\ln[t_1\nu(n+1)]}-1\right\}}. \quad (21)$$

If the dissociation energy does not vary with cluster size, then

$$F_n=(3n-6)\left[\frac{1}{\ln(t_1\nu n)}-\frac{1}{\ln(t_2\nu n)}\right] \quad (22)$$

which can be also expressed as

$$F_n=(3n-6)\,\frac{k^2T_1T_2}{D^2}\ln\left(\frac{t_2}{t_1}\right), \quad (23)$$

where T_1 and T_2 are deduced from Eqs. (14), (18) and Eqs. (16), (18), respectively. The dissociation ratio roughly increases as $(3n-6)$ following an universal law which only indicates that clusters are formed from an evaporative ensemble. As Gspann proposed,[17] if one assumes that the De-

TABLE I. Dissociation energies associated to the following dissociation channels; $Li_n^+ \rightarrow Li_{n-1}^+ + Li$ $D_{n,1}^+$; $Li_n^+ \rightarrow Li_{n-2}^+ + Li_2$ $D_{n,2}^+$, obtained from unimolecular evaporation rates and using the fitting procedure described in the text.

n	$D_{n,1}^+$ (eV)	$D_{n,2}^+$ (eV)
5		1.4
6	1.20	
7	1.34	1.48
8	1.03	1.31
9	1.60	1.57
10	0.83	1.37
11	1.30	1.07
12	1.04	1.28
13	1.20	1.18
14	1.09	1.23
15	1.23	1.26
16	1.08	1.25
17	1.22	1.24
18	1.14	1.30
19	1.31	1.39
20	1.16	1.41
21	1.35	1.45
22	1.04	1.33
23	1.21	1.19
24	1.11	1.26
25	1.20	1.25
26	1.14	1.28
27	1.17	1.25
28	1.15	1.26
29	1.19	1.28
30	1.16	1.29
31	1.18	1.28
32	1.17	1.29
33	1.22	1.33
34	1.18	1.34
35	1.24	1.36
36	1.20	1.38
37	1.22	1.36
38	1.22	1.38
39	1.23	1.39
40	1.20	1.37
41	1.24	1.38
42	1.15	1.33

bye frequency varies by less than one order of magnitude with the nature of the element, a scaling between D and $T = \sqrt{T_1 T_2}$ can be inferred.

With our experimental device $t_1 = 0.18\sqrt{n}$ μs and $t_2 = 3.68\sqrt{n}$ μs. Using the characteristic vibrational frequency for lithium $\nu = 8\times10^{12}$ Hz estimated from Debye capacity model[18] Eq. (22) surprisingly well accounts for the general trend of F_n vs cluster size as shown in Fig. 3(a).

The local deviations from the universal law permit the relative values of the dissociation energies to be obtained [Eq. (21)]. To go further one needs an energy constraint. In the case of alkali clusters we use the cycle obtained from the two evaporative channels

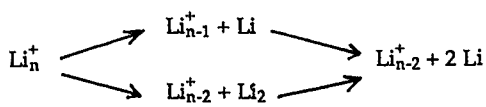

Energy balance requires

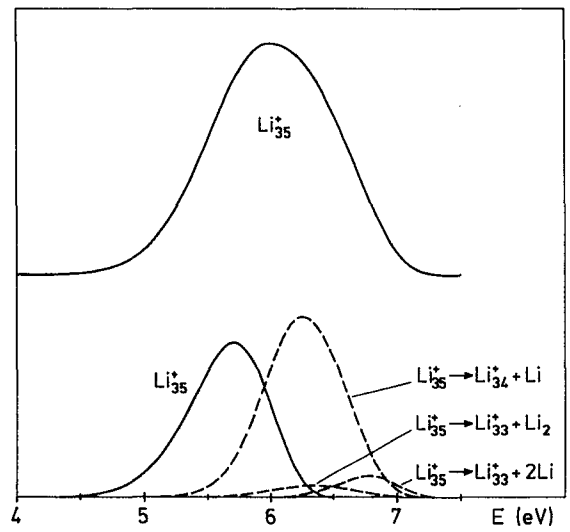

FIG. 5. Distribution of internal energy of mass selected packet Li_{35}^+ at t_1 (upper trace). The lower trace shows the probabilities for the different fragmentation channels to occur against the internal energy of the parent.

$$D_{n,1}^+ + D_{n-1,1}^+ = D_{n,2}^+ + D_2, \tag{25}$$

where $D_{n,1}^+$ and $D_{n,2}^+$ are the dissociation energies for monomer and dimer evaporation, respectively, and D_2 the dissociation energy of Li_2 taken from Ref. 19 as $D_2 = 1.056$ eV. Thus, if the monomer and dimer evaporation channels for the n-mer have equal dissociation energies then

$$D_{n-1,1}^+ = D_2. \tag{26}$$

In a first step dissociation energies are roughly determined from this procedure which combines metastable evaporation rates and energy constraints. We verified that the dissociation energies obtained for homogeneous clusters, depend very little on the choice of the statistical theory used for the evaluation of the rate constants. In fact, it is well known that the absolute values of dissociation rates require the exact density of states, which remains an unresolved issue for clus-

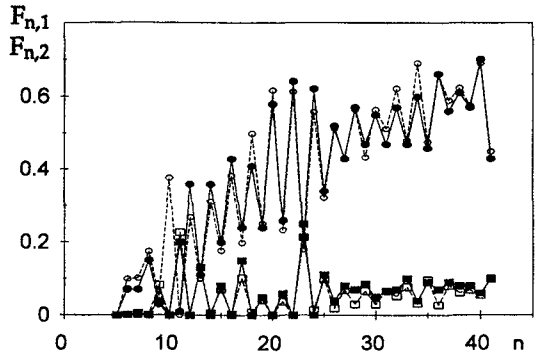

FIG. 6. Fractional dissociation ratios $F_{n,1}$ (dots) and $F_{n,2}$ (squares) [see Eqs. (1) and (2)] as a function of cluster size. The full dots and squares denote experimental values, the open circles and squares denote calculated values from Eqs. (28) and (29). The experimental value for mass 10 is missing due to dimer evaporation of mass 11.

TABLE II. Comparison between experimental dissociation energies and CI *ab initio* predictions (Ref. 22) and Hückel calculations.

	Experiments (this work)		CI *ab initio* calculations[a]		Hückel calculations	
n	$D^+_{n,1}$ (eV)	$D^+_{n,2}$ (eV)	$D^+_{n,1}$ (eV)	$D^+_{n,2}$ (eV)	$D^+_{n,1}$ (eV)	$D^+_{n,2}$ (eV)
2	1.30[c]		1.23			
3	1.50[d]		1.43	1.77	1.89	
4	0.8[e]		0.64	1.18	0.80	1.63
5		1.40[e]	1.26	1.01	1.67	1.41
6	1.20		0.95	1.32	1.00	1.61
7	1.34	1.48	1.49	1.54	1.58	1.52
8	1.03	1.31	0.65	1.25	1.04	1.56
9	1.60	1.57	1.41[b]	1.25[b]	1.81	1.79
10	0.83	1.37	0.23[b]	0.9[b]	0.81	1.56

[a]Reference 22.
[b]Values obtained with a smaller basis set (Ref. 33).
[c]$D^+_2 = D_2 + \mathrm{IP(Li)} - \mathrm{IP(Li_2)}$ with D_2 taken from Ref. 19, IP(Li)=5.39 eV, IP(Li_2) taken from Ref. 20.
[d]Reference 21.
[e]These values are given with an error bar of 0.1 eV, whereas $D^+_{n,1}$ and $D^+_{n,2}$ with $n>5$ are given with an error bar of 0.05 eV.

ters, and that RRK theory underestimates the dissociation rates by several orders of magnitude. However the unimolecular decay of clusters formed from a well defined evaporative ensemble implies evaporation within two successive time windows, i.e., $[0,t_1]$ and $[t_1,t_2]$. The fractional dissociation ratio, between the two time windows depends on the relative variation of the density of states from one size to its precursor which varies little with the statistical theory chosen.

In a second step dissociation energies are determined from the resolution of the rate equations taking into account two steps for monomer evaporation and one for dimer evaporation, both for the formation of Li_n^+ cluster packet during t_1 and for its evaporation during t_2-t_1. The probability $Q(n,E,t_1)$ that Li_n^+ contains at t_1 an internal energy E is obtained from Eqs. (10), (11), (12),

$$Q(n,E,t_1)=A[P^{(1)}_{0,t_1}(n+2,E+D^+_{n+2,2},n)+P^{(2)}_{0,t_1} \times(n+2,E+D^+_{n+2,1}+D^+_{n+1,1},n)], \quad (27)$$

where A is a normalization factor. After the unimolecular decay of Li_n^+ during the time t_2-t_1 the relative abundance of Li^+_{n-1} and Li^+_{n-2} fragments are

$$F_{n,1}=\frac{\int_0^\infty Q(n,E,t_1)P^{(1)}_{t_1t_2}(n,E,n-1)dE}{\int_0^\infty Q(n,E,t_1)dE}, \quad (28)$$

$F_{n,2}$

$$=\frac{\int_0^\infty Q(n,E,t_1)[P^{(1)}_{t_1,t_2}(n,E,n-2)+P^{(2)}_{t_1,t_2}(n,E,n-2)]dE}{\int_0^\infty Q(n,E,t_1)dE}. \quad (29)$$

As an example, the energy distribution of the selected *packet* Li^+_{35} at t_1 which will partially dissociates at t_2 for giving

$$\begin{aligned} Li^+_{35} &\rightarrow Li^+_{34}+Li \\ &\rightarrow Li^+_{33}+Li_2 \\ &\rightarrow Li^+_{33}+Li+Li \end{aligned} \quad (30)$$

is represented with the different contributions in Fig. 5.

In order to determine cluster binding energies we used RRK rate constants. Taking into account the energy constraint of Eq. (26) and using $D^+_{n,1}$ and $D^+_{n,2}$ as fitting parameters we vary their values in order to achieve optimum agreement with measured fractional intensity ratios $F_{n,1}$, $F_{n,2}$. The best fit is plotted in Fig. 6. The corresponding dissociation energies are given in Table I. Since monomer and dimer evaporations often coexist, the energy constraint of Eq. (25), taking D_2 as 1.056 eV,[19] permits the dissociation energies to be bracketed with an uncertainty less than 0.05 eV except for Li_5^+ for which the unimolecular dissociation rate is low. Moreover only dimer evaporation occurs for Li_5^+ leading to an upper limit on $D^+_{4,1}$ of $D^+_{4,1}<0.85$ eV.

E. Beyond two step evaporative process

For larger cluster sizes, the number of successive evaporations which occur during the observational time window t_2-t_1 increases leading to a less precise determination of the dissociation energies. The best approach to measuring dissociation energies of large clusters is to photoexcite a mass selected cluster packet Li_n^+ with a known amount of energy $h\nu$ and to observe the fragmentation pattern corresponding to the sequential loss of monomers within a given time window Δt. However in order to avoid incorrect conclusions because of the difficulty of knowing the internal energy of the cluster parent before excitation, the parents are heated up to reach the temperature defined by the time window Δt. We have previously shown[6] that in such conditions the mean value of the dissociation energy over an evaporative sequence is $h\nu/p$, where p is the number of lost atoms during the time window Δt.

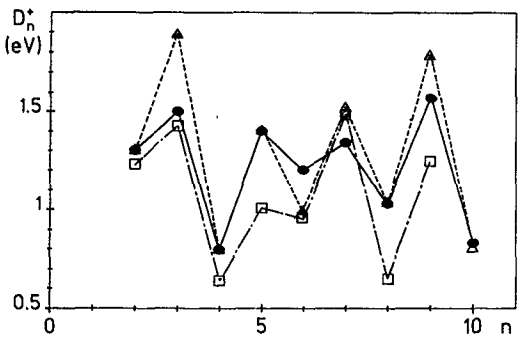

FIG. 7. Lowest dissociation energies inferred from fractional dissociation ratios for $4 \leq n \leq 10$ as well as the experimental values deduced from Refs. 19,20,21 for Li_2^+ and Li_3^+ (dots) together with CI *ab initio* calculations from Ref. 22 (open squares) and our Hückel type calculations assuming the same geometries as Na_n^+ (Ref. 23) (open triangles).

V. DISCUSSION

A. Dissociation energies

The experimental values of the dissociation energies of small Li_n^+ obtained from Refs. 19,20,21 for Li_2^+ and Li_3^+ and from our measurements for Li_n^+ with $4 \leq n \leq 10$ are compared with the CI energies of cationic lithium clusters obtained for SCF optimized structures by Bonacic–Koutecky *et al.*[22] and with our Hückel type calculations for Li_n^+ with Hückel parameter $\beta = D_2/2 = 0.53$ eV using the same geometries as Na_n^+ (Ref. 23) (Table II). The lowest dissociation energies are reported in Fig. 7. Odd–even alternation is present both for the measured and the calculated dissociation energies obtained for the most stable structures of Li_n^+. However the difference between the predicted and the measured dissociation energies can reach 0.4 eV. The amplitude of the odd–even alternation is overestimated in the Hückel calculations,

TABLE III. Comparison of amplitude ratios of shell closing at $n=9$ and $n=21$ for K (Ref. 6), Na (Ref. 5), and Li (this work).

	K	Na	Li
$\frac{D_9^+ - D_{10}^+}{D_9^+}$	0.44	0.56	0.47
$\frac{D_{21}^+ - D_{22}^+}{D_{21}^+}$	0.25	>0.30	0.23

and the small gap which has been measured between the dissociation energies of Li_5^+ and Li_6^+ is better described by *ab initio* CI calculations.

The lowest dissociation energies of Li_n^+ clusters with $3 \leq n < 42$ are reported in Fig. 8 together with the previous measurements on Na_n^+ (Ref. 5) and K_n^+.[6] Superimposed on an odd–even alternation, they present similar sawtooth behavior that is well understood in the framework of the electron shell model.[24] The sharp drops after ion cluster masses 9, 21, and to a certain extent after 35 for Na_n^+ and 41 for Li_n^+ correspond to electron configuration shell closings of 8, 20, 34, and 40 electrons. Both odd–even alternation and shell closing amplitudes decrease as the cluster size increases. The odd–even alternation, corresponding to relatively more stable cluster with even number of electrons, is more pronounced for Li_n^+ than for K_n^+ and Na_n^+. It is then interesting to compare quantitatively the amplitude ratios of shell closings of 8 and 20 electrons, taken as $(D_9^+ - D_{10}^+)/D_9^+$ and $(D_{21}^+ - D_{22}^+)/D_{21}^+$, for the three alkalies, potassium, sodium, and lithium. From these ratios (Table III) it is clear that the shell closings are more pronounced for Na_n^+ than for K_n^+ in agreement with a more pronounced electronic shell behavior for sodium than for potassium in the jellium model. In fact for the same number of electrons, the cluster radius of Na_n^+ is smaller than that of K_n^+. The corresponding potential well is

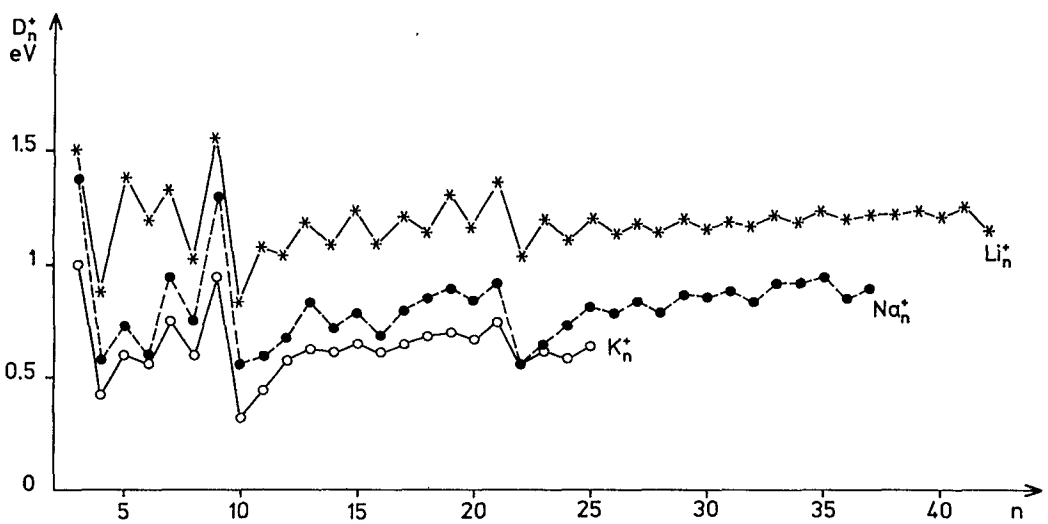

FIG. 8. Dissociation energies of the lowest dissociation channel for K_n^+ (Ref. 6), Na_n^+ (Ref. 5) and Li_n^+ (present work) vs n. The sawtooth behavior is clearly seen for the three cases.

TABLE IV. Comparison between the cohesive energy per atom for neutral and ionic clusters obtained from our experimental data and the CI *ab initio* predictions (Ref. 21). Notice that the calculated values lead to less bound clusters than experimental ones.

	$E_T(Li_n^+)/n$ (eV)		$E_T(Li_n)/n$ eV	
n	exp	CI	exp	CI
2	0.65	0.62	0.53	0.45
3	0.93	0.89	0.50	0.45
4	0.90	0.83	0.63	0.63
5	1.05	0.91	0.78	0.65
6	1.08	0.92	0.88	0.72
7	1.11	1.00	0.91	0.78
8	1.10	0.96	0.95	0.80

deeper for Na_n^+ than for K_n^+ and the space between two levels is larger for Na_n^+ than for K_n^+. Following the jellium model, Li_n^+, which has a cluster radius smaller than Na_n^+, should exhibit a more pronounced shell behavior in contrast with the experimental results. This is consistent with the failure of the jellium model to describe photoexcitation spectra of lithium clusters[25] without taking into account ionic structure effects.[26–27] The enhanced odd–even alternation for Li_n^+ as compared to that of Na_n^+ and K_n^+ could reflect a greater degree of covalent bonding in Li_n^+.

B. Cohesive energies

For studying the evolution to the bulk it is more convenient to convert the dissociation energies into cohesive energies per atom for neutral clusters. First the measured ionic dissociation energies are converted into the total cohesive energy E_T of Li_n^+ for $n \leqslant 42$,

$$E_T(Li_n^+) = \sum_{k=2}^{k=n} D_{k,1}^+ . \tag{31}$$

For $42 < n < 100$ the total cohesive energy is obtained from photoevaporation experiments (IV-5).

The total cohesive energy of neutral Li_n is obtained from the thermodynamic cycle

$$\begin{array}{ccc} Li_n & \rightarrow & nLi \\ \downarrow & & \downarrow \\ Li_n^+ & \rightarrow & (n-1)Li+Li^+ \end{array} \tag{32}$$

as

$$E_T(Li) = E_T(Li_n^+) + IP(Li_n) - IP(Li), \tag{33}$$

where IP stands for the ionization potential. Using the experimental ionization potentials available up to $n=26$ (Ref. 9) we deduce the cohesive energy for Li_n.

For small sizes, $n \leqslant 8$ the cohesive energies per atom, i.e., $E_T(Li_n^+)/n$ and $E_T(Li_n)/n$ of ionic and neutral species, respectively, are compared with CI *ab initio* calculations of Bonacic–Koutecky *et al.*[22] in Table IV. Although the general experimental trends are well predicted by CI calculations, the cohesive energies per atom from the *ab initio* calculations are all systematically lower than the experimental data.

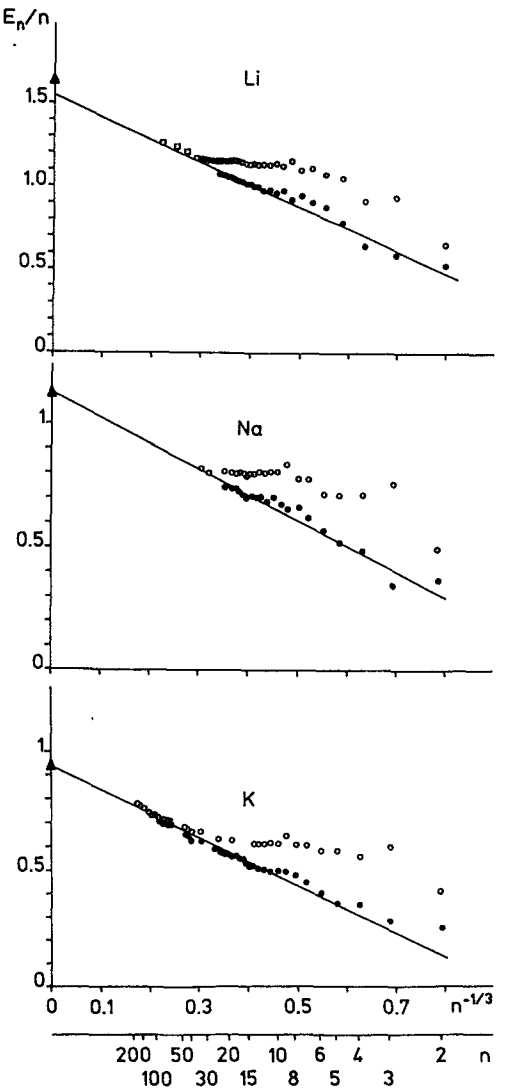

FIG. 9. Plot of cohesive energies per atom for neutral () and ionic () clusters against $n^{-1/3}$ for lithium, sodium, and potassium. The cohesive energies of neutral species fall onto straight lines $a_v - a_s n^{-1/3}$ leading to experimental determination of a_v and a_s. Triangles are the bulk cohesive energies.

In Fig. 9 we plot the cohesive energies per atom against $n^{-1/3}$, a value proportional to the fraction of surface atoms in the cluster, together with our previous results on sodium[5] and potassium.[6] The cohesive energies per atom of ionic clusters are larger than that of neutrals. The difference between these energies per atom is $[IP(Li) - IP(Li_n)]/n$ [see Eq. (33)]. The metallic behavior implies an ionization energy smaller for clusters than for the atom leading to an increase of stability for ionic species. However $[IP(Li) - IP(Li_n)]/n$ is less than 3% for $n > 100$ and tends to zero as n goes to infinity. The cohesive energy per atom of neutral clusters fall onto a straight line

$$\frac{E_T(Li_n)}{n} = a_v - a_s n^{-1/3} \tag{34}$$

in agreement with a classical model, which assumes that the

TABLE V. a_v and a_s coefficients deduced from the cluster experiment and compared to bulk values taken from Refs. 29–31 for a_v, and from Miedema's determination for a_s (Ref. 28).

(eV)		Li	Na	K
a_v (exp)		1.52	1.12	0.94
Cohesive energy				
solid		1.62	1.13	0.94
liquid		1.53	1.01	0.80
a_s (exp)		1.3	1.02	0.98
$4\pi r_a^2\gamma(T=0)$		1.23	0.91	0.78
a_s/a_v	(exp)	0.85	0.91	1.04
	bulk	0.76	0.81	0.83

total cohesive energy of an n-atom cluster is equal to the volume energy $a_v n$ of n volume atoms minus the energy $4\pi r_a^2 n^{2/3}\gamma$ to break bounds and to create the cluster surface. Hence a_v is the cohesive energy per atom and a_s is related to the surface energy γ as

$$a_s = 4\pi r_a^2 \gamma, \tag{35}$$

where r_a is the radius of one atom deduced from the molar volume. In Table V we compare the coefficients a_v and a_s deduced from our experimental cluster data with the most reliable bulk values from Miedema[28] for lithium, sodium, and potassium.

The values a_v for the cohesive energy per atom deduced from our cluster measurements well agree with the bulk sublimation energies for Na and K and with the bulk vaporization energies for Li.[29,30,31] Since the difference between sublimation and vaporization energies is less than 10% it is difficult to conclude from this comparison if the clusters are liquid or solid. Concerning the a_s coefficients, the values deduced from cluster measurements are slightly larger than those estimated by Miedema[28] at $T=0$, but the agreement is better for lithium than for sodium and potassium. Following Rose *et al.* it is interesting to know if the universal features of bonding in metals[32] also account for metallic clusters. For example if the surface binding energy can be approximately expressed in terms of the bulk quantities[30] as

$$4\pi r_s^2 \gamma = 0.82 a_v . \tag{36}$$

The a_s/a_v ratios are given in Table V showing that Eq. (36) is verified within 20%.

C. Cluster temperature

Using the microcanonical definition of the temperature of a finite system of n elements as

$$T = \frac{E}{k(3n-6)} \tag{37}$$

the energy distribution of a cluster packet is converted into temperature distribution. Using binding energies the distribution of internal energy is determined for each mass selected cluster packet entering the time of flight. However as been noted, the dissociation energies are well defined provided that the energy constraint is known, but the deduced internal energy distribution depends on the chosen statistical theory and a shift of 20% to 30% can be expected in the whole. Figure 10 shows the temperature distributions for cluster sizes $5 \leqslant n \leqslant 42$ using RRK theory. The characteristic shell closing discontinuities at $n=9,21$ are clearly observed. The increased stability at the shell closing permits the cluster to support relatively more internal energy per mode than it is possible for the new opening shell. Since the width of the internal energy distribution is roughly independent of cluster size, the width of the temperature distribution decreases as cluster size increases. For large cluster sizes a temperature of 720 K can be defined for all clusters which is substantially larger than their melting point.

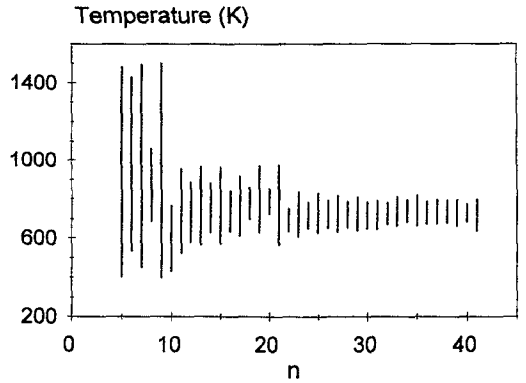

FIG. 10. Temperature distribution corresponding to internal energy per mode as a function of cluster size. The bars correspond to FWHM of $Q(n,E,t_1)$ from Eq. (27).

VI. CONCLUSION

In this work unimolecular dissociation of energy rich Li_n^+ is used to determine the dissociation pathways and bond energies for monomer and dimer evaporation. Accurate dissociation values can be obtained if we account for the energy constraint which connects monomer and dimer evaporative channels. Binding energies of the lowest dissociation channels are found to follow a sawtooth behavior less pronounced than it should be from the extrapolation of potassium and sodium cluster data. The average cohesive energies per atom for neutral clusters deduced from our measurements on cluster ions and the literature ionization potentials evolve as expected from the universal features of bonding in metals from small sizes. The average cohesive energies per atom for small cluster ions deviate from the linear behavior of neutrals showing an increase of stability for ionic species due to charge solvation.

[1] P. J. Robinson and K. A. Holbrook, *Unimolecular Reactions* (Wiley, London, 1972); W. Forst, *Theory of Unimolecular Reactions* (Academic, New York, 1973).
[2] A. J. Stace and A. K. Shukla, Chem. Phys. Lett. **85**, 157 (1982).
[3] C. Klots, J. Chem. Phys. **83**, 5854 (1985), Z. Phys. D **5**, 83 (1987).
[4] See, for examples, C. X. Su, D. A. Hales, and P. B. Armentrout, J. Chem. Phys. **99**, 6613 (1993), and references therein; M. Sowa, P. Hintz, and S. Anderson, *ibid.* **95**, 4719 (1991).
[5] C. Bréchignac, Ph. Cahuzac, J. Leygnier, and J. Weiner, J. Chem. Phys. **90**, 1492 (1989).

[6] C. Bréchignac, Ph. Cahuzac, F. Carlier, M. de Frutos, and J. Leygnier, J. Chem. Phys. **93**, 7449 (1990).
[7] H. Haberland, H. Kornmeier, H. Langosch, M. Oschwald, and G. Tanner, J. Chem. Soc. Faraday Trans. **86**, 2473 (1990).
[8] M. Jarrold and E. Honea, J. Phys. Chem. **95**, 9185 (1991).
[9] Ph. Dugourd, D. Rayane, P. Labastie, B. Vezin, J. Chevaleyre, and M. Broyer, Chem. Phys. Lett. **197**, 433 (1992).
[10] C. Bréchignac, Ph. Cahuzac, F. Carlier, M. de Frutos, and J. Ph. Roux, Phys. Rev. B **47**, 2271 (1993).
[11] W. C. Wiley and I. H. Mac Laren, Rev. Sci Instrum. **26**, 1150 (1955).
[12] P. Scheier and T. D. Märk, Phys. Rev. Lett. **59**, 1813 (1987); Chem. Phys. Lett. **148**, 393 (1988).
[13] O. K. Rice and H. C. Ramsperger, J. Am. Chem. Soc. **49**, 1617 (1927).
[14] L. S. Kassel, J. Phys. Chem. **32**, 225 (1928); **32**, 1065 (1928).
[15] R. A. Marcus and O. K. Rice, J. Phys. Colloid Chem. **55**, 894 (1951); R. A. Marcus, J. Chem. Phys. **20**, 359 (1952).
[16] V. Weisskopf, Phys. Rev. **52**, 295 (1937).
[17] J. Gspann, in *Physics of Electronic and Atomic Collisions*, edited by S. Datz (North–Holland, Amsterdam, 1982), pp. 79–96.
[18] N. W. Ashcroft and N. D. Mermin, in *Solid State Physico* (Holt Saunder, Tokyo, 1981), p. 461.
[19] J. Vergès, R. Bacis, B. Barakat, P. Carrot, S. Churassy, and P. Crozet, Chem. Phys. Lett. **98**, 203 (1983).
[20] R. Bernheim, L. Gold, and T. Tipton, J. Chem. Phys. **78**, 3635 (1983).
[21] C. H. Wu, J. Chem. Phys. **65**, 3181 (1976).
[22] V. Bonacic-Koutecky, J. Gaus, M. F. Guest, L. Cespiva, and J. Koutecky, Chem. Phys. Lett. **206**, 528 (1993).
[23] D. M. Lindsay, Y. Wang, and T. F. George, J. Chem. Phys. **86**, 3493 (1987).
[24] W. Ekardt, Phys. Rev. B **29**, 1558 (1984).
[25] C. Bréchignac, Ph. Cahuzac, J. Leygnier, and A. Sarfati, Phys. Rev. Lett. **70**, 2036 (1993).
[26] S. Blundell and C. Guet, Z. Phys. B **28**, 81 (1993).
[27] L. Serra, G. B. Bachelet, N. Van Giai, and E. Lipparini, Phys. Rev. B (in press).
[28] A. Miedema, Z. Metall. **69**, 287 (1978).
[29] C. Kittel, in *Introduction of Solid State Physics* (Wiley, New York, London, Sydney, 1966).
[30] J. Perdew, Phys. Rev. B **37**, 6175 (1988).
[31] *JANAF Thermochemical Tables*, 3rd ed. (American Chemical Society, New York, 1985), Vol. 14.
[32] J. Rose, J. Smith, and J. Ferrante, Phys. Rev. B **28**, 1835 (1983); J. Rose, J. Vary, and J. Smith, Phys. Rev. Lett. **53**, 344 (1984).
[33] I. Boustani, W. Pewestorf, P. Fantucci, V. Bonacic-Koutecky, and J. Koutecky, Phys. Rev. B **35**, 9437 (1987).